Proceedings of the 17th World Congress
The International Federation of Automatic Control
Seoul, Korea, July 6-11, 2008

# Identification of Intra-Cellular Feedback Loops by Intermittent Step Perturbation Method

**Chao-Yi Dong[1,2], Kwang-Hyun Cho[3*], Tae-Woong Yoon[4]**

*1. School of Electrical Engineering, Korea University, Seoul, 136-713, Korea*
*(E-mail: dongchaoyi@korea.ac.kr).*
*2. School of Information and Engineering, Inner Mongolia University of Technology, Huhhot, 010051, China*
*3. Department of Bio and Brain Engineering and KI for the BioCentury,*
*Korea Advanced Institute of Science and Technology (KAIST), Daejeon, 305-701, Korea*
*(*Corresponding author, Tel: +82-42-869-4325; Fax: +82-42-869-4310; E-mail: ckh@kaist.ac.kr)*
*4. School of Electrical Engineering, Korea University, Seoul, 136-713, Korea*
*(Co-correspondence, E-mail: twy@korea.ac.kr)*

**Abstract:** Feedback loops play pivotal roles in the regulation and control of many important cellular processes such as gene transcription, signal transduction, and metabolism. Hence, identification of feedback loops embedded in biomolecular regulatory networks is crucial to understanding the regulatory mechanisms underlying various cellular processes. In this paper, we introduce an identification method called the intermittent step perturbation method (ISPM) that can efficiently identify and locate feedback connectivities among reacting biomolecules. In particular, a sort of stochastic function called an intermittent step perturbation is applied to excite a given network. Then, we employ a statistical algorithm to analyze the resulting time-series data, thereby discerning any causal connection with a circular causal property. This circular causal property implies the existence of a feedback loop in the regulatory network. Finally, the proposed ISPM is demonstrated through an insulin signal transduction pathway model.

## 1. INTRODUCTION

Feedback loops play a crucial role in various functioning of intracellular networks. A large number of experiments indicated that positive feedback loops dominate diverse cellular processes including development, cell proliferation, apoptosis, and the response to stress (Eisen *et al*., 1967; Wolpert and Lewis, 1975), whereas negative feedback loops contribute to maintaining homeostasis of a biological system under some internal and external changes (Wolf and Heinrich, 2000; Strogatz, 2000; Maeda *et al*., 2004; Laub and Loomis, 1998; Thomas and Kaufman, 2001). Therefore, the identification of feedback loops and the understanding of feedback regulation mechanism are central themes in systems biology research.

Although some methods for identification of feedback loops were reported in the literature, they have fundamental limitations in application to biological networks. For instance, Vance (Vance *et al*., 2002) utilized impulse responses based on time-series data, but feedback loops could not be distinguished from feedforward regulations. The likelihood ratio test method (LRTM) proposed by Caines and Chan (1975) was suitable to identify the existence of feedback loops, but it was confined only to the stationary stochastic processes and required detailed *a priori* knowledge on the system order and structure. The acquisition of such *a priori* knowledge is very difficult in practice, particularly for lage regulatory networks. Hence, there is a pressing need to develop a more efficient identification method which can overcome such disadvantages of previous methods.

In this paper, we propose a novel identification method called the intermittent step perturbation method (ISPM). The main idea is to identify underlying feedback loops by investigating their causal properties. Note that a biomolecular regulatory network can be represented by a directed graph where nodes indicate biomolecules and the directed edges connecting two nodes indicate the corresponding causal relationships. A prominent characteristic of a feedback loop is that it corresponds to a sequential causal regulatory chain in which every node can be affected by all the other nodes. Such a particular property of a feedback loop is referred as a 'circular causality' here. To investigate the circular causality in an intracellular regulatory network, we apply a particular perturbation - an intermittent step perturbation. Then, time-series data of each network node are obtained and a statistical correlation analysis is used to infer causal connections in the network. Once we unravel all the connectivities with the circular causality, we can identify the existence of feedback loops and can locate their structures within the regulatory network.

## 2. METHODS

### *2.1 The nonlinear dynamics of intracellular networks subject to perturbations*

The dynamic behavior of an intracellular network can be described as a set of nonlinear differential equations:

$$d\mathbf{x}/dt = \mathbf{f}(t, \mathbf{x}, \boldsymbol{\lambda}) + \mathbf{u} \quad (1)$$

where

- $n$ is the number of state variables;
- $\mathbf{x}(t)$ is the $n$ dimensional state vector;
- $\mathbf{f}$ is the $n$ dimensional vector field describing the nonlinear dynamics of the network;
- $\boldsymbol{\lambda}$ is the $p$ dimensional parameter vector;
- $\mathbf{u}$ is the $n$ dimensional input vector.

In this intracellular network, the state $\mathbf{x}(t)$ represents the concentrations or activity levels of the network nodes (i.e., the reacting biomolecules); $n$ denotes the number of the network nodes; $\boldsymbol{\lambda}$ denotes external or internal conditions such as rate constants, pH values, and temperatures (as the nominal interaction structure of a network is considered time-invariant, $\boldsymbol{\lambda}$ is assumed to be constant); $\mathbf{u}$ represents perturbations such as impulse, step, ramp, sinusoid, or stochastic perturbations. We postulate that such perturbations can be realized by an active substance release under control and they are applied to each node one by one in the form of an input rather than a parameter. Hence, the inherent interaction structure is not affected by such external perturbations and is solely determined by $\mathbf{f}$ and its parameters $\boldsymbol{\lambda}$.

### *2.2 The definition of feedback loops*

The concept of feedback loop stems from the Jacobian matrices of the above system descriptions in (1). Suppose that the function vector $\mathbf{f}$ is continuously differentiable in its biologically feasible domain, then the Jacobian matrix $\mathbf{A}$ at the state $\mathbf{x}^*(t) = (x_1^*, x_2^*, .....x_n^*)$ is defined as $\mathbf{A}\big|_{\mathbf{x}^*} = \left.\frac{\partial \mathbf{f}}{\partial \mathbf{x}}\right|_{\mathbf{x}^*}$.

If the element $\frac{\partial f_i}{\partial x_j}$ of the Jacobian matrix $\mathbf{A}$ is nonzero (or significantly larger than zero in its absolute value), then this implies that $x_j$ has an interaction with $x_i$. In particular, we can conjecture the existence of a feedback loop if some components of the system interact with one another in a circular manner. Thus, in the Jacobian matrix, each set of nonzero elements corresponding to a feedback loop has the same row and column index set (Thomas and Kaufman, 2001). The sign of the feedback loop can be further determined by $(-1)^q$ where $q$ is the number of negative interactions in the feedback loop (Thomas and Kaufman, 2001).

### *2.3 The causality attribute table for identifying the existence of a feedback loop*

Based on the concepts of nonlinear cellular dynamics and feedback loops, we develop a circular causality criterion to judge the existence of a feedback loop. Fig. 1 illustrates how the criterion helps identify a circular causal connectivity in a simple synthetic biomolecular regulatory network. First, we perturb each node one by one. For the $i$th perturbation ($i = 1, 2, 3...n$), the concentration changes of all nodes are recorded in the $i$th row of Table 1, where the nonzero concentration change implies a causal interaction from the perturbed node. Then, the sign 'V' is assigned to denote this causal interaction in Table 1, and the sign 'O' is assigned to denote no causal interaction when the concentration change of one node is zero. Since the information in Table 1 exhibits the causal interactions among the network nodes, we call this table causality attribute table (CAT) to highlight such characteristics. In particular, the main diagonal sub-block full of 'V's in the CAT correspond to the existence of a feedback loop. As observed in Table 1, node 2, 3, and 4 form such a main diagonal sub-block, and a feedback loop composed of these three nodes is denoted by the shadow region. Consequently, based on the distribution of causal interactions, we can identify and locate the feedback loops in the CAT systematically.

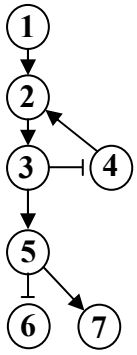


**Fig. 1.** A 7-node synthetic pathway network. The 'arrows' denote 'activating regulations' and the 'line-bars' denote 'inhibiting regulations'.

**Table 1.** The CAT corresponding to Figure 1. The shadow region indicates a feedback loop including node 2, 3, and 4.

| | 1 | 2 | 3 | 4 | 5 | 6 | 7 |
|---|---|---|---|---|---|---|---|
| 1 | V | V | V | V | V | V | V |
| 2 | O | **V** | **V** | **V** | V | V | V |
| 3 | O | **V** | **V** | **V** | V | V | V |
| 4 | O | **V** | **V** | **V** | V | V | V |
| 5 | O | O | O | O | V | V | V |
| 6 | O | O | O | O | O | V | O |
| 7 | O | O | O | O | O | O | V |

### *2.4 The design of perturbations and the identification algorithm*

In addition to utilizing the circular causal property, another key idea of our identification algorithm is to apply an intermittent step perturbation which can fully excite a given intracellular network. This perturbation scheme is based on recent technological advancements. For instance, we can think of the flash photolysis technology that has been rapidly developed in cell biology and biochemistry over the last decade (Corrie *et al*., 1992; Nerbonne, 1986). According to the flash photolysis technology, the incorporation and photolysis of caged proteins or peptides into living cells can

be realized through controlled flash impulse sequences. Thus, aided by the flash impulse sequences, we can perturb intracellular networks and delineate their kinetics in a very delicate way (Adams and Tsien, 1993). Besides this flash photolysis technology, we can think of other perturbation schemes. We note that control inputs are often approximated by modulated high frequency impulse sequences in control engineering. So, we can photolyze some amount of caged proteins with a high frequency flash impulse sequence to approximate any desired perturbation profile. For example, in Fig. 2 we illustrate how a sinusoid function can be approximated by a high frequency flash impulse sequence. Thus, an intermittent step input (see Fig. 3) which is controlled according to a random triggering (Hull and Dobell, 1962) can also be approximately obtained by the same method. Such an intermittent step input can be commonly considered as a stochastic signal uncorrelated with any intrinsic noise and other unknown external inputs. Therefore, the perturbation is particularly suitable to attenuating the influence of external unknown inputs through correlation computations. This is to be taken as the main perturbation method in this paper.

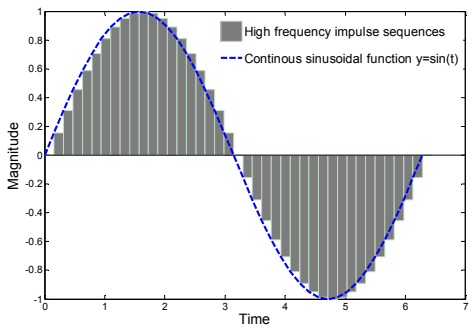


**Fig. 2.** A sinusoid function approximated by a high frequency flash impulse sequence.

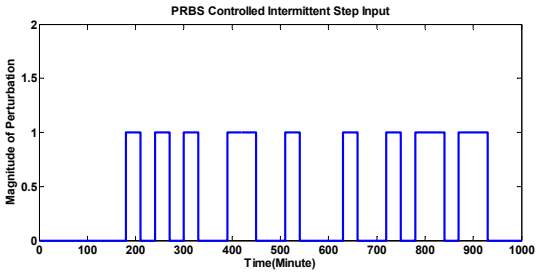


**Fig. 3.** The intermittent step input. The magnitude =1.

### *2.5 Correlation coefficient method*

Although the CATs can help detect feedback loops efficiently, many factors such as measurement noises and unexpected interactions from the outer environment may hinder deducing the CATs correctly. So, a quantitative method called correlation analysis is employed to facilitate evaluating strengths of the causal connections and further to obtain the appropriate CATs. The correlation coefficient $\rho_{xy}$ between two normalized time-series $x(t)$ and $y(t)$ can be defined by the following equations.

$$\rho_{xy} = \frac{1}{m}\sum_{i=1}^{m}\left(\frac{x(t_i)-\bar{x}}{\sigma_x}\right)\left(\frac{y(t_i)-\bar{y}}{\sigma_y}\right) \tag{3}$$

$$\sigma_x = \sqrt{\frac{1}{m}\sum_{i=1}^{m}\left(x(t_i)-\bar{x}\right)^2}\,;\sigma_y = \sqrt{\frac{1}{m}\sum_{i=1}^{m}\left(y(t_i)-\bar{y}\right)^2} \tag{4}$$

$$\bar{x} = \frac{1}{m}\sum_{i=1}^{m}x(t_i);\bar{y} = \frac{1}{m}\sum_{i=1}^{m}y(t_i) \tag{5}$$

where

$m$ is the number of sample points.

$\bar{x}$ is the mean value of time-series $x(t_i)$, and $\bar{y}$ for $y(t_i)$.

$\sigma_x$ is the sample standard deviation of time-series $x(t_i)$, and $\sigma_y$ for $y(t_i)$.

As correlations in time-series data reveal dependencies between variables, these correlations can be used to infer the connectivity between biomolecular species (Eisen *et al.*, 1998; Rice *et al.*, 2005). However, although correlation-based approaches provide quantitative estimates on the connectivity between biomolecular species, the correlation does not necessarily deduce causality. To discern the pseudo causal connections among correlation connections, Arkin and Ross (Arkin and Ross, 1995) decomposed correlation connections into four scopes: (i) direct antecedent connections (node 1 and node 2 in Fig. 1), (ii) indirect antecedent connections (node 1 and node 3 in Fig. 1), (iii) direct or indirect common antecedent connections (node 6 and node 7 in Fig. 1), (iv) unanalyzed connections from the externally controlled variables. These cases explained all possible correlation connections between biomolecular species, but only the first two cases can be regarded as causal connections. The other two cases may induce false positives, considering the possibilities that high correlations might happen in these cases. Hence, we developed the two techniques to identify the false positive cases. The first technique is to perturb all network nodes in turn and to extract only the *i*th row with *i* being the index of perturbation) in the *i*th correlation coefficient matrix. This helps discern the common antecedent connections from the real causal connections. The second technique which is the intermittent step perturbations can contribute to excluding the unanalyzed outer connections from inner causal connections. Based on the two proposed techniques, the CATs of intracellular network can be obtained by comparing the derived correlation coefficients with a specified threshold value. If the correlation coefficient is above the threshold value $\rho_T$, it is concluded that a causal connection exists between two nodes. Such a threshold value is set as 0.3 during our studies. Finally, we summarize the complete algorithm for feedback identification in Fig. 4.

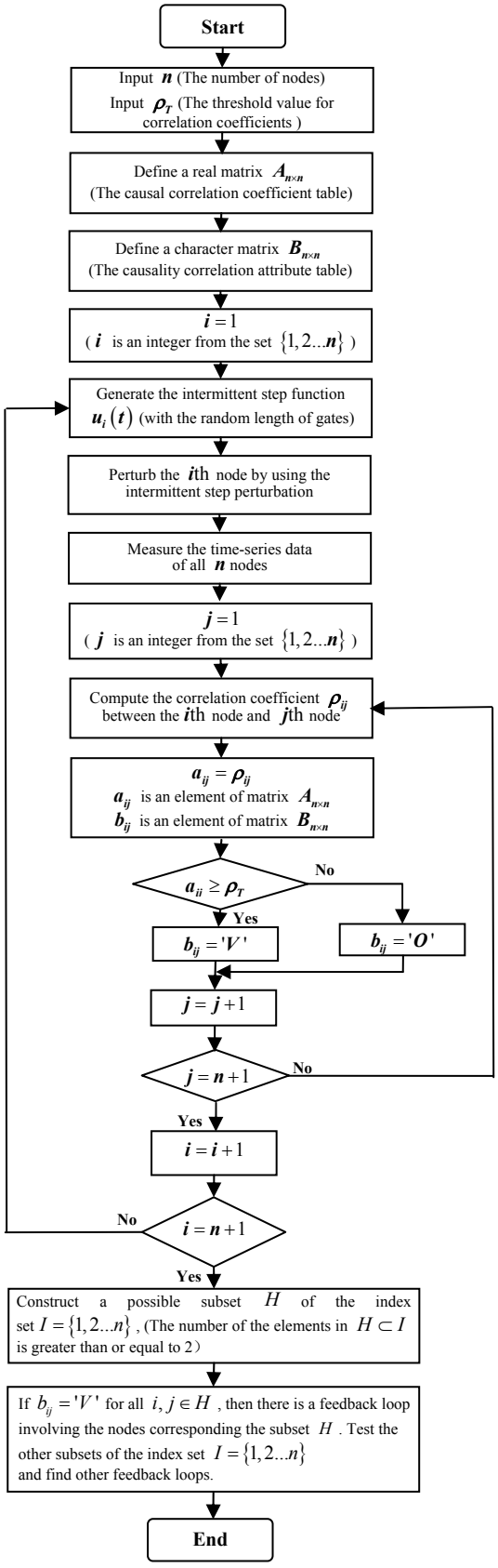


**Fig. 4.** Feedback loop identification algorithm

## 3. RESULTS

A biological example of the insulin signal transduction pathway model is used to illustrate the ISPM. The signaling through the insulin pathway is critical for regulation of blood glucose levels and for avoidance of diabetes. Many modeling processes of the signal transduction pathway were widely discussed in the literature (De Fea and Roth, 1997; Paz, 1999; Ravichandra *et al*., 2001a,b). More recently, a relatively complete mathematical model was constructed to further elucidate the feedback regulatory mechanisms of the insulin signal transduction pathway (Sedaghat *et al*., 2002). The dotted lines in Fig. 5 indicate the four feedback loops in this model as follows:

(i) Positive feedback loop from Akt ( $x_{17}$ ) to IRS-1 ( $x_{10}$ )

(ii) Positive feedback loop from Akt ( $x_{17}$ ) to the phosphorylated one bound surface receptors ( $x_5$ ) .

(iii) Positive feedback loop from Akt ( $x_{17}$ ) to the phosphorylated two bound intracellular receptors ( $x_7$ ) and the phosphorylated one bound intracellular receptors ( $x_8$ ) .

(iv) Negative feedback loop from PKC-$\xi$ ( $x_{19}$ ) to the serine-phosphorylated IRS-1 ( $x_{22}$ ).

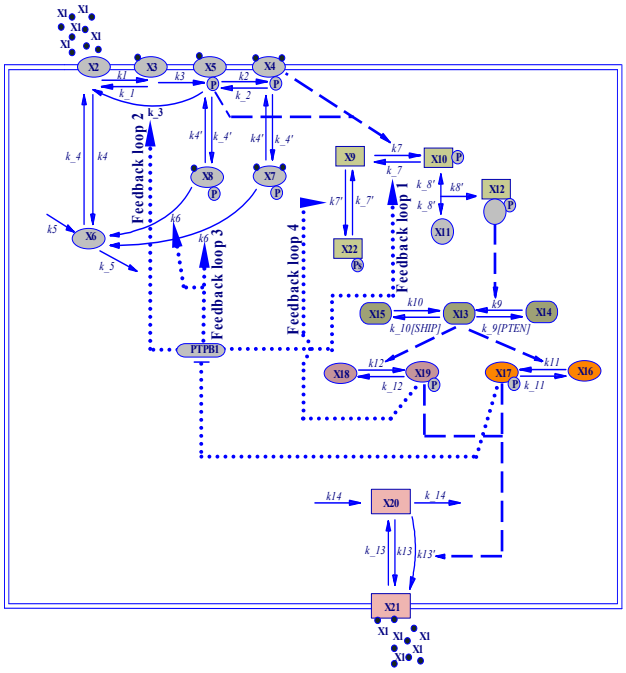


**Fig. 5.** The diagram of the insulin signal transduction pathway with 4 feedback loops. The solid lines denote the substance fluxes in the pathway, and the dashed lines indicate the indirect control to the downstream nodes. The dotted lines from activated Akt ( $x_{17}$ ) to PTPB1 represent the feedback loops 1, 2, and 3. The dotted lines from PKC-$\xi$ ( $x_{19}$ ) to IRS-1 ( $x_9$ ) represent the feedback loop 4.

where $x_1$ is the insulin input; $x_2$ is the concentration of unbound surface insulin receptors; $x_3$ is the concentration of unphosphorylated one bound surface receptors; $x_4$ is the concentration of phosphorylated two bound surface

receptors; $x_5$ is the concentration of phosphorylated one bound surface receptors; $x_6$ is the concentration of unbound unphosphorylated intracellular receptors; $x_7$ is the concentration of phosphorylated two bound intracellular receptors; $x_8$ is the concentration of phosphorylated one bound intracellular receptors; $x_9$ is the concentration of unphosphorylated IRS-1; $x_{10}$ is the concentration of tyrosine-phosphorylated IRS-1; $x_{11}$ is the concentration of unactivated PI 3-kinase; $x_{12}$ is the concentration of tyrosine-phosphorylated IRS-1/activated PI3-kinase complex; $x_{13}$ is the percentage of PI(3,4,5)P3 out of the total lipid population; $x_{14}$ is the percentage of PI(4,5)P2 out of the total lipid population; $x_{15}$ is the percentage of PI(3,4)P2 out of the total lipid population; $x_{16}$ is the percentage of unactivated Akt; $x_{17}$ is the percentage of activated Akt; $x_{18}$ is the percentage of unactivated PKCξ; $x_{19}$ is the percentage of activated PKCξ; $x_{20}$ is the percentage of intracellular GLUT4; $x_{21}$ is the percentage of cell surface GLUT4; $x_{22}$ is the concentration of serine-phosphorylated IRS-1.

First, we apply the intermittent step perturbations with a minimum time interval of 30 minutes to excite the pathway, so that the downstream biomolecular species can fully response to the perturbation happening in the upstream nodes. The magnitude of each step input is determined by its effect to the cell surface GLUT4. To guarantee that the intracellular network always stay in its linear operation region, we limit the perturbation magnitudes to the extent that the perturbations can make the percent of cell surface GLUT4 increase to the half of its maximum concentration (40%). The time-series data of all nodes are sampled at every 10 minutes, and 10% Guassian measurement noises are mixed with those data to mimic the real biological experiments. Then, the causal correlation coefficient tables and their corresponding CATs can be obtained by using the algorithm in Fig. 4.

**Table 2.** The CAT of four feedback loops (threshold level for correlation coefficient is 0.3).

| | X1 | X2 | X3 | X4 | X5 | X6 | X7 | X8 | X9 | X1 | X1 | X1 | X1 | X1 | X1 | X1 | X1 | X2 | X2 | X2 |
|---|---|---|---|---|---|---|---|---|---|---|---|---|---|---|---|---|---|---|---|---|
| X1 | V | V | V | V | V | O | V | V | V | V | O | V | V | O | V | O | V | V | V | V | V | V |
| X2 | O | V | V | V | V | V | V | V | V | V | O | V | V | O | V | O | V | O | V | V | V | V |
| X3 | O | V | V | V | V | O | V | V | V | V | O | V | V | O | V | O | V | O | V | V | V | V |
| X4 | O | O | O | V | V | O | V | O | V | V | O | V | V | O | V | O | V | O | V | O | V | V |
| X5 | O | V | V | V | V | O | V | V | V | V | O | V | V | O | V | O | V | O | V | V | V | V |
| X6 | O | V | V | V | V | V | V | V | V | V | O | V | V | V | V | V | V | V | V | V | V | V |
| X7 | O | V | V | V | V | V | V | V | V | V | O | V | V | O | V | O | V | O | V | V | V | V |
| X8 | O | V | V | V | V | V | V | V | V | V | O | V | V | O | V | O | V | O | V | V | V | V |
| X9 | O | O | O | V | V | O | V | V | V | V | O | V | V | O | V | V | V | V | V | V | V | V |
| X1 | O | O | O | V | V | O | V | V | V | V | O | V | V | O | V | O | V | O | V | V | V | V |
| X1 | O | O | O | V | V | O | V | V | V | V | V | V | V | O | V | O | V | O | V | V | V | V |
| X1 | O | O | O | O | V | O | V | V | V | V | V | V | V | O | V | O | V | O | V | V | V | V |
| X1 | O | O | O | V | V | O | V | V | V | V | O | V | V | V | V | O | V | O | V | V | V | V |
| X1 | O | O | O | V | V | O | V | V | V | V | O | V | V | V | V | O | V | O | V | V | V | V |
| X1 | O | O | O | V | V | O | V | V | V | V | O | V | V | O | V | V | V | O | V | V | V | V |
| X1 | O | O | O | V | V | O | V | V | V | V | O | V | V | O | V | O | V | V | V | V | V | V |
| X1 | O | O | O | V | V | O | V | V | V | V | O | V | V | O | V | O | V | V | V | V | V | V |
| X2 | O | O | O | O | O | O | O | O | O | O | O | O | O | O | O | O | O | O | O | V | V | O |
| X2 | O | O | O | O | O | O | O | O | O | O | O | O | O | O | O | O | O | O | O | V | V | O |
| X2 | O | O | O | V | V | O | V | V | V | V | O | V | V | O | V | V | V | V | V | V | V | V |

Aided by the intermittent step perturbations, the statistical correlation analysis of time-series data correctly captures the causal correlations of the pathway. The CAT of the feedback loop model is shown in Table 2 where the sign 'V's indicate the causal connections in the network. The result shows that most of interaction hierarchies in Table 2 are consistent with those of the pathway model. Some direct bidirectional reactions ( $x_{13}$ , $x_{14}$ , and $x_{15}$ ), ( $x_{20}$ and $x_{21}$ ), ( $x_{18}$ and $x_{19}$ ), and ( $x_{16}$ and $x_{17}$ ) can be founded in Table 2. More importantly, the feedback loops also emerge after extracting some relevant rows and columns from Table 2.

The feedback loop ( $x_{10}$ , $x_{12}$ , $x_{13}$ , $x_{17}$ , and $x_{19}$ ) is identified after extracting corresponding (10, 12, 13, 17, and 19th) rows and columns from Table 2. Thus, the feedback loops 1 and 4 are both correctly identified. Similarly, the ( $x_4$ , $x_5$ , $x_9$ , $x_{10}$ , $x_{12}$ , $x_{13}$ , and $x_{17}$ ), i.e. , the feedback loop 2 can be identified from Table 3. However, the feedback loop 3 ( $x_7$ , $x_8$ , $x_4$ , $x_5$ , $x_{10}$ , $x_{12}$ , $x_{13}$ , and $x_{17}$ ) fails to be identified. To investigate this failure, we study the ODE of the mathematical model. Some relatively faint regulations take place due to the small value of the parameter $k_6$ . Therefore, the measurement noises dwarf this faint deterministic causal connection and as a result affect the identification result.

**Table 3.** The identification of the feedback loop 2

| | X1 | X4 | X5 | X9 | X10 | X12 | X13 | X17 | X19 | X21 |
|---|---|---|---|---|---|---|---|---|---|---|
| X1 | V | V | V | V | V | V | V | V | V | V |
| X4 | O | V | V | V | V | V | V | V | V | V |
| X5 | O | V | V | V | V | V | V | V | V | V |
| X9 | O | V | V | V | V | V | V | V | V | V |
| X10 | O | V | V | V | V | V | V | V | V | V |
| X11 | O | V | V | V | V | V | V | V | V | V |
| X12 | O | V | V | V | V | V | V | V | V | V |
| X13 | O | V | V | V | V | V | V | V | V | V |
| X17 | O | V | V | V | V | V | V | V | V | V |
| X19 | O | O | O | V | V | V | V | V | V | V |
| X21 | O | O | O | O | O | O | O | O | O | V |

## 4. DISCUSSION

With the help of the correlation analysis, the ISPM provides an efficient approach for rapidly identifying and locating intracellular feedback loops without *a priori* knowledge on the biomolecular network architectures. The simulation shows that the method is robust to the high levels of measurement noises, scalable for larger biochemical networks, and is efficient for nonlinear cellular dynamics. With the advances in experimental perturbation technologies and high throughput measurement methods, it may soon be applicable to transcriptional, protein, and metabolic interaction networks.

Besides identifying the feedback loops, the ISPM also retrieves plenty of causal information which is contained in

the CATs. We note that a positive coefficient $\rho_{ij}$ in causal correlation coefficient tables indeed indicates a direct or indirect activation from the *i*th node to the *j*th node and likewise a negative coefficient for an inhibitory regulation. Therefore, such implicit information provides a possibility to deduce more detailed intracellular interaction architectures by collecting the information of the distribution of causality in the CATs.

The ISPM postulates all biomolecular species accessible for direct perturbations. This requirement cannot however always be fulfilled *in vivo*. To overcome this disadvantage, the experiments can be designed among those perturbable network nodes. Nevertheless, ISPM is still helpful in detecting and validating the existence of feedback loops. In addition, we further need to account of the time-delays present in biomolecular causal connections to simplify analysis. The time-delays are often caused by transcription, translation, or post-translational modification in the intracellular environment. They may affect the correlation analysis, and even can cause a false positive. To resolve this problem, we can employ previous works (Adams and Tsien, 1993; Cho *et al*., 2006) suggesting some efficient measures. The key idea of these studies is shifting one time-series data in time axis while keeping the other time-series data fixed. When the maximum value of correlation coefficient is reached, the pure time-delay can be estimated by the shifting time. Therefore, despite all these limitations, the proposed method still suggests an efficient way to detect feedback loops in intracellular biomolecular network.

## ACKNOWLEDGMENT

This work was supported by the Korea Science and Engineering Foundation (KOSEF) grant funded by the Korea government (MOST) (M10503010001-07N030100112) and also supported from the Korea Ministry of Science and Technology through the Nuclear Research Grant (M20708000001-07B0800-00110) and the 21C Frontier Microbial Genomics and Application Center Program (Grant MG05-0204-3-0).

## REFERENCES

A.Arkin, J.Ross (1995). Statistical construction of chemical-reaction mechanisms from measured time-series. *J. Phys. Chem.*, **vol. 99**, pp. 970–979.

A.R.Sedaghat, A.Sherman and M.J.Quon (2002). A mathematical model of metabolic insulin signaling pathways. *Am. J. Physiol Endocrinol Metab.*, **vol. 283**, pp. 1084-1101.

H.Eisen, P.Brachet, L.Pereira da Silva and F.Jacob (1967). Regulation of repressor inhibition in lambda. *Proc. Natl. Acad. Sci.,* **vol. 66**, pp. 855–862.

J.E.T.Corrie, Y.Katayama, G.P.Reid, M.Anson, D.R. Trentham (1992). The development and application of photosensitive caged compounds to aid time-resolved structure determination of macromolecules. *Philos. Trans. R. Soc. London Ser.*, **A vol. 340**, pp. 233-243.

J.J.Rice, Y.H.Tu and G.Stolovitzky (2005). Reconstructing biological networks using conditional correlation analysis. *Bioinformatics*, **vol. 21**, N. 6, pp. 765-773.

J.M.Nerbonne (1986). Design and application of photolabile intracellular probes. *Soc. Gen. Physiol. Ser.*, **vol.40**, pp. 417-45.

J.Wolf and R.Heinrich (2000). Effect of cellular interaction on glycolytic oscillations in yeast: a theoretical investigation. *Biochem J.,* **vol. 345**, pp. 321-334.

K.DeFea and R.A.Roth (1997). Protein kinase C modulation of insulin receptor substrate-1 tyrosine phosphorylation requires serine 612. *Biochemistry*, **vol. 36**, pp. 12939–12947.

K.-H.Cho, J.-R.Kim, S.Baek, H.-S.Choi, and S.-M.Choo (2006). Inferring Biomolecular Regulatory Networks from Phase Portraits of Time-Series Expression profiles. *FEBS Letters*, **vol. 580**, pp. 3511-3518.

K.Paz, Y.F.Liu, H.Shorer, R.Hemi, D.LeRoith, M.Quon, H.Kanety, R.Seger and Y.Zick (1999). Phosphorylation of insulin receptor substrate-1 (IRS-1) by protein kinase B positively regulates IRS-1 function. *J. Biol. Chem.*, **vol. 274**, pp. 28816–28822.

L.V.Ravichandran, H.Chen, Y.Li, and M.J.Quon (2001a). Phosphorylation of PTP1B at Ser(50) by Akt impairs its ability to dephosphorylate the insulin receptor. *Mol. Endocrinol*, **vol. 15**, pp. 1768–1780.

L.V.Ravichandran, D.L.Esposito, J.Chen, and M.J.Quon (2001b). Protein kinase C-ξ phosphorylates insulin receptor substrate-1 and impairs its ability to activate phosphatidylinositol 3-kinase in response to insulin. *J. Biol. Chem.*, **vol. 276**, pp. 3543–3549.

L.Wolpert and J.H.Lewis (1975). Towards a theory of development. *Fed. Proc.*, **vol. 34**, pp. 14–20.

M.B.Eisen, P.T.Spellman, P.O.Brown and D.Botstein (1998). Cluster analysis and display of genome-wide expression patterns. *Proc. Natl. Acad. Sci. USA*, **vol. 95**, pp. 14863–14868.

M.Maeda, Lu.Sijie, G.Shaulsky, Y.Miyazaki, H.Kuwayama, Y.Tanaka, A.Kuspa and W.F.Loomis (2004). Periodic signaling controlled by an oscillatory circuit that includes protein kinase ERK2 and PKA. *Science*, **vol. 304**, pp. 875-878.

M.T.Laub and W.F.Loomis (1998). A molecular network that produces spontaneous oscillations in excitable cells of dictyostelium. *Molecular Biology of the Cell*, **vol. 9**, pp. 3521-3532.

R.Thomas and M.Kaufman (2001). Multistationarity, the basis of cell differentiation and memory. I. Structural conditions of multistationarity and other nontrivial behavior. *Chao,* **vol. 11**, pp. 170-179.

S.H.Strogatz (2000). From Kuramoto to Crawford: Exploring the onset of synchronization in populations of coupled oscillations. *Physica D.*, **vol. 143**, pp. 1-20.

S.R.Adams and R.Y.Tsien (1993). Controlling cell chemistry with caged compounds. *Annu. Rev. Physiol.* , **vol. 55**, pp. 755-84.

T.E.Hull, and A.R.Dobell (1962). Random Number Generater *Soc. Indust. Appl. Math. Rev.*, **vol. 4**, pp. 230-254.

W.Vance, A.Arkin, J.Ross (2002). Determination of causal connectivities of biomolecular species in reaction networks. *Proc. Natl. Acad. Sci. USA,* **vol. 99**, pp. 5816–5821.

P.E. Caines and C.W. Chan, (1975). Feedback between stationary stochastic processes. IEEE Trans AC. **vol.** 20, pp. 498-508.